Journal of Modern Physics, 2013, 4, 1-7
http://dx.doi.org/10.4236/jmp.2013.47A2001 Published Online July 2013 (http://www.scirp.org/journal/jmp)

Thermal Modeling of Cylindrical $LiFePO_4$ Batteries

Mojtaba Shadman Rad[1,2], Dmitri L. Danilov[1], Morteza Baghalha[2], Mohammad Kazemeini[2], Peter H. L. Notten[1,3*]

[1]Department of Chemistry and Chemical Engineering, Eindhoven University of Technology, Eindhoven, The Netherlands
[2]Chemical & Petroleum Engineering Department, Sharif University of Technology, Tehran, Iran
[3]Department of Electrical Engineering, Eindhoven University of Technology, Eindhoven, The Netherlands
Email: *P.H.L.Notten@TUE.nl

Received May 4, 2013; revised June 6, 2013; accepted July 3, 2013

ABSTRACT

Thermal management of Li-ion batteries is important because of the high energy content and the risk of rapid temperature development in the high current range. Reliable and safe operation of these batteries is seriously endangered by high temperatures. It is important to have a simple but accurate model to evaluate the thermal behavior of batteries under a variety of operating conditions and be able to predict the internal temperature as well. To achieve this goal, a radial-axial model is developed to investigate the evolution of the temperature distribution in cylindrical Li-ion cells. Experimental data on $LiFePO_4$ cylindrical Li-ion batteries are used to determine the overpotentials and to estimate the State-of-Charge-dependent entropies from the previously developed adaptive thermal model [1]. The heat evolution is assumed to be uniform inside the battery. Heat exchange from the battery surfaces with the ambient is non-uniform, *i.e.* depends on the temperature of a particular point at the surface of the cell. Furthermore, the model was adapted for implementation in battery management systems. It is shown that the model can accurately predict the temperature distribution inside the cell in a wide range of operating conditions. Good agreement with the measured temperature development has been achieved. Decreasing the heat conductivity coefficient during cell manufacturing and increasing the heat transfer coefficient during battery operation suppresses the temperature evolution. This modified model can be used for the scale-up of large size batteries and battery packs.

Keywords: Lithium-Ion Batteries; Thermal Modeling; Entropy; Energy; Electrochemistry; Heat Transfer

1. Introduction

A successful design of battery packs starts with the correct accommodation of the thermal battery properties. Using high thermally resistant materials, such as binders in the electrodes and polymer separators is inevitable in constructing high performance batteries, but this limits the heat transfer inside the cells. Consequently, higher temperatures are expected at the core of the cells compared to its surface. However high temperatures are not permitted for safety and reliability reasons; they can accelerate battery degradation and even cause thermal runaway. In a battery management system (BMS), it is desirable to accurately predict the internal temperature evolution of the battery according to the state-of-charge (SOC), cell potential, current and surface temperature. Such a system requires an efficient thermal model with a limited number of measured parameters at each state. Therefore heat dissipation in a cell must be properly studied in order to avoid elevated temperatures where decomposition reactions of the electrodes and electrolyte are started [2].

A number of models have been developed to study the thermal behavior of Li-ion or Li-polymer batteries [1,3-22]. Theoretical models, which are usually based on a combination of electrochemistry and physics, can give accurate predictions for various operating conditions [3-10]. But these are complicated and need sophisticated measurements and estimation of transport properties, electrochemical reaction constants, etc. to be accurately solved. Such models are well-suited for battery design purposes, though not optimal for the low computing-power environment of micro-controllers used in BMS [20]. On the other hand, experimental-based models employ battery measurements on the cell level to determine equilibrium potentials and, consequently, overpotentials and in some studies, entropy contributions in heat generation, but do not go into detail of the electrochemical processes occurring inside the cells [1,11-18,22].

The present paper represents combination of both ap-

*Corresponding author.

proaches. An experimental-based methodology for accurate two-dimensional thermal modeling of cylindrical cells is proposed. Commercially available high power 2.3 Ah $LiFePO_4$ batteries, which are an interesting option for hybrid electrical vehicles (HEVs) and full electrical vehicles (EVs), are used in this study. Previously developed lumped thermal model [1] is implemented for this cell chemistry to provide part of the input data of the two-dimensional model based on the experimental data and then for extension of the model. In the previous work, it was shown how one can explicitly determine the equilibrium potentials by polynomial extrapolation towards zero current, and obtain the overpotentials at various currents and SoC. Then a back-estimation method was introduced to find the values of the entropy changes from the adapted thermal model.

The main challenge and contribution of this work is to implement a proper two-dimensional model of heat dissipation by using overpotentials and temperature derivatives of the equilibrium potentials, which gives a proper rate of the heat generation. The developed model is exported into Matlab, enabling a user-friendly implementation into a BMS. COMSOL multiphysics is used for finite element modeling, and then the model is exported to MATLAB for estimation of the various parameters.

2. Theoretical Considerations

2.1. Model Development

Based on the differential energy balance in cylindrical coordinates, the following heat transport partial differential equation (PDE) is obtained

$$\rho C_p \frac{\partial T}{\partial t} = \frac{k}{r}\frac{\partial}{\partial r}\left(\frac{\partial T}{\partial r}\right) + k\frac{\partial^2 T}{\partial z^2} + H^{in}(t,r,z), \qquad (1)$$

where ρ is the density [g·m^{-3}], C_p the specific heat capacity [J·g^{-1}·K^{-1}], T the temperature [K], t time [s], k the thermal conductivity [W·m^{-1}·K^{-1}], r radial coordinate and z is the axial coordinate. Note that derivatives with respect to θ, the tangential coordinate, are absent since the considered problem possesses radial symmetry. The heat source term $H^{in}(t,r,z)$ [W·m^{-3}] includes all battery processes that contributes to the heat evolution, according to

$$H^{in}(t,r,z) = \frac{H_\eta(t) + H_s(t,r,z)}{V_C}, \qquad (2)$$

where $H_\eta(t)$ [W] represents the overpotential heat, $H_s(t,r,z)$ [W] the entropic heat and V_C [m^3] is the volume of the battery.

$$H_\eta(t) = \eta_t(t) I(t), \qquad (3)$$

where the overpotential $(\eta_t(t))$ [V] is defined as the difference between equilibrium cell potential (E_{eq}) and the operating cell potential (E)

$$\eta_t(t) = E(t) - E_{eq}(t), \qquad (4)$$

$\eta_t(t)$ is always defined positive during charging and negative upon discharging. $I(t)$ [A] specifies the current flowing through the individual electrodes which is by definition positive during charging and negative upon discharging. So $H_\eta(t)$ is always positive. $H_s(t,r,z)$ is the entropic heat [W] which can be represented by

$$H_s(t,r,z) = I(t)T(t,r,z)\frac{\Delta S(t)}{nF}, \qquad (5)$$

where n is the number of electrons that are transferred in the electrochemical reaction during the battery operation and F is the Faraday constant [96,486 C·mol^{-1}]. $\Delta S(t)$ [J·mol^{-1}·K^{-1}] expresses the entropy change of the individual electrochemical charge transfer reaction during battery operation and has been derived at our previous work [1], according to

$$\Delta S(t) = nF\left(\frac{\partial E_{eq}}{\partial T}\right)_{\xi,P}, \qquad (6)$$

where ξ represents, in general terms, the reaction progress, in our specific case the SoC of the cell. The initial condition for the partial differential equation (Equation (1)) for the whole cell is

$$T(0,r,z) = T_a, \qquad (7)$$

where T_a [K] is the ambient temperature. Denoting the radius of the cell as R and length of the cell as L energy conservation requires that on the surface of the cell there is a balance between heat conduction and sum of convection and radiation heat transfer, according to

$$-\boldsymbol{n}\cdot(k\nabla T) = h(T - T_a) + \sigma\varepsilon\left(T^4 - T_a^4\right), \qquad (8)$$

where h is the average convective heat transfer coefficient [W·m^{-2}·K^{-1}] between the cell and the environment, σ = 5.67 × 10^{-8} [J·s^{-1}·m^{-2}·K^{-4}] is the Stefan-Boltzmann constant and ε is the emissivity factor of the surface material. ∇T represents temperature gradient and $\boldsymbol{n}$ is the outer normal vector of unit length.

2.2. Experimental

2.3 Ah cylindrical A123 (ANR26650m1) $LiFePO_4$ cells were investigated in this study. Temperature development as a function of applied current, potential and operating regime was recorded. The experimental data were used to determine the overpotential and SoC-dependent entropy changes and to validate the thermal model. Cycling was performed with an 8-channel MACCOR 4000 battery tester. The temperature development was measured on the middle of the surface of the cell by the potential drop across PT100 type thermo-resistors connected to

battery tester via the auxiliary potential input. A water bath was used to control the ambient temperature in a climate control box (**Figure 1**). To evaluate the thermal behavior of the cells, three different temperatures were investigated: 0˚C, 20˚C and 40˚C.

Constant current-constant voltage (CCCV) charging was applied in this study. Charging was carried out at 1.6 A (= 0.7 C-rate) till the maximum cell potential of 3.6 V was attained. Charging was continued under constant voltage conditions at 3.6 V until the charging current dropped below 0.3 A (End-of-Charge). Subsequently, CCCV-charging was followed by a relaxation period of 180 min. Constant current (CC) was then applied to discharge the battery at various C-rates. Discharging was terminated at 2.0 V. The following rated currents were employed for discharging: 0.05, 0.10, 0.15, 0.20, 0.30, 0.50, 0.75, 1.00, 1.50 and 2.00 C-rates.

2.3. Model Parameters and Assumptions

The battery specifications are summarized in **Table 1**. The battery consists of several components: organic electrolyte, dissolved lithium salts, polymer separator, current collectors, graphite and composite electrodes, supporting materials, metal casing, etc. So it is difficult to estimate the overall physical properties of the cell based on the physical properties of its constituents. **Table 2** provides some proposed and estimated values of required physical properties of the main cell components.

Surface emissivity factor (ε) of the batteries is assumed to be 0.65. The small observed variation in E_{eq} upon battery aging is neglected. Considering heat capacities of the components, the average heat capacity of the cells is estimated to be 1.36 [J·g^{-1}·K^{-1}].

Considering natural convection of air around a horizontally positioned cylinder, the following expression has been adopted for the heat transfer coefficient [23]

$$Nu_f = \frac{hd}{k_{amb}} = 0.36 + \frac{0.518Ra^{1/4}}{\left[1+\left(0.559/\Pr\right)^{9/16}\right]^{4/9}}, \quad (9)$$

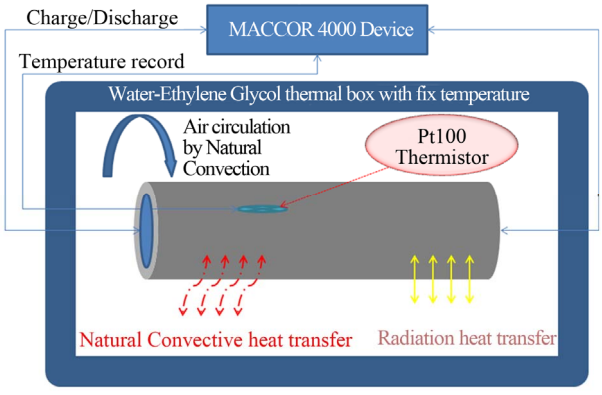

Figure 1. Experiment set-up.

Table 1. Battery specifications.

Parameter	Value or description
Diameter	25.85 mm
Height	65.15 mm without terminals
Mass	Approx. 70 g
Positive Electrode	$LiFePO_4$
Negative Electrode	Porous Graphite
Nominal Capacity	2.3 Ah at 0.2 C

Table 2. Physical properties of the cell components.

	Cell (Avg.)	Separator (PP)	Cathode	Anode
C_P [J·g^{-1}·K^{-1}]	1.36	1.93-2.00	1.25	1.20
k [W·m^{-1}·K^{-1}]	0.4	0.12-0.22	0.4	1.4
ρ [g·m^{-3}]	2.047·10^6	9.02 - 9.06·10^5	2.208·10^6	1.410·10^6

where Nu_f is the average dimensionless Nusselt number, h is the average natural (free) convection heat transfer coefficient [W·m^{-2}·K^{-1}], d the diameter of the battery [m] and k_{amb} is thermal conductivity of air [W·m^{-1}·K^{-1}]. Ra is the dimensionless Rayleigh number, defined as $Ra = Gr_D \cdot \Pr$ in which Gr_D is the dimensionless Grashof number, $Gr_D = \frac{g\beta(T-T_a)D^3}{\upsilon^2}$ and $\Pr = \frac{C_p\mu}{k}$ is the Prandtl number, g [m·s^{-2}] is the gravity constant, β [K^{-1}] is the volumetric thermal expansion coefficient, which is defined as $1/T_a$ for ideal gases. Parameters μ and υ represent the viscosity and kinematic viscosity of air, respectively.

3. Results and Discussion

The thermal behavior of the batteries has been evaluated up to 2C-discharge rates at ambient temperature 20˚C. The results at this temperature are presented here as a common ambient temperature for the battery operations in electrical vehicles. However the battery measurements and simulation have also been performed at 0˚C and 40˚C to determine equilibrium potentials and derive entropy change values to further validation of the model.

3.1. EMF, Overpotential and Entropy Determination

The measured cell potentials during cycling with various discharge C-rates at 20˚C are shown in **Figure 2(a)**. The battery is charged to 3.6 V according to the standard charging regime in every cycle. During the subsequent 3 hours of relaxation under open-circuit conditions, the cell potential drops to about 3.4 V, after that discharging

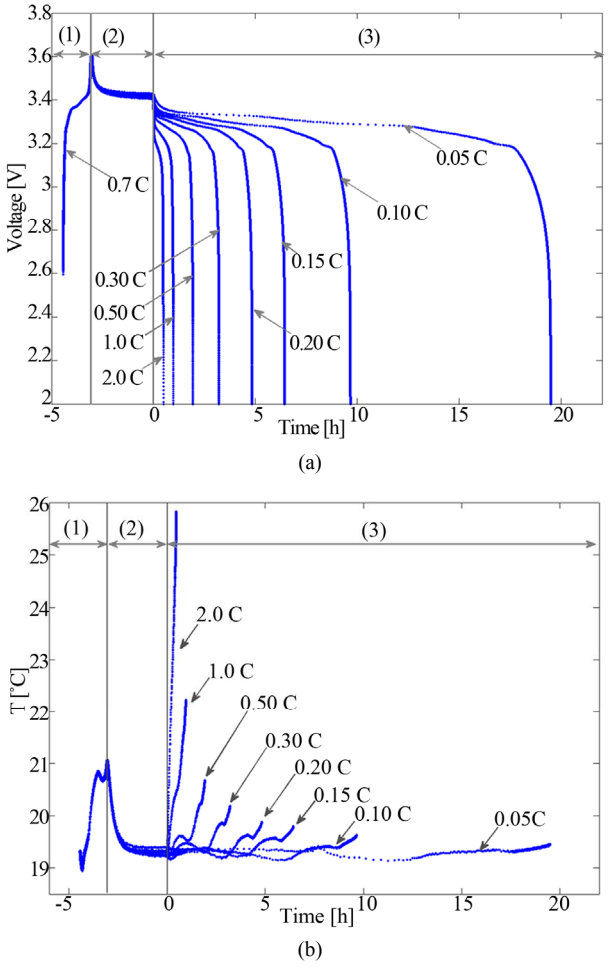

Figure 2. (a) Cell potential development during charging (1), relaxation (2) and discharging (3) at various C-rates and (b) the corresponding temperature development. Ambient temperature is 20˚C.

starts. The discharge cut-off potential is 2 V. **Figure 2(b)** represents the temperature development during cycling. It is clearly visible that the temperature evolution becomes more pronounced at higher C-rates. The temperature normally increases during (dis)charging. However at some specific stages the temperature decreases. Since the overpotential heat is always positive, this can be explained only by a negative entropic heat contribution, which will be discussed later.

The methodology developed in previous work [1] is used to determine the overpotentials and SoC-dependent entropy changes from the experimental data. Modeling starts with estimation of the equilibrium potential. Extrapolation of the measured cell potential towards 0 C-rate discharge current which has introduced in the previous works is used to determine the equilibrium potentials [1,24,25]. **Figure 3** shows the measured potential curves, the determined E_{eq} dependence (black upper potential curve) and the overpotential curves (insert).

According to Equation (4) the overpotential can be obtained from the EMF and the cell potential discharge curves (see inset of **Figure 3**). The as-determined overpotentials serve as important input parameter to calculate the heat evolution Equation (3). Another heat contribution (see Equation (4)) is related to the entropy. In order to reduce the complexity of the calculations 11 Q_{out}-regions are considered. Values of ΔS in 11 subsequent nodes of the discrete grid, *i.e.* SoC from 0 to 1 with step 0.1 are treated as unknown optimizing parameters. These ΔS values are determined from an optimization procedure by a lumped thermal model based on battery measurements [1], considering the best agreement between experimentally measured and theoretical evolution of the surface cell temperature as criteria. Optimization has been performed across 10 cycle of (dis)charge as the cell measurements have been performed. ΔS values as a function of SoC are displayed in **Figure 4**. The obtained values for entropy changes are in consistence with the reported values for this battery by C. Forgez *et al*. [20].

3.2. 2D-Model

It is assumed, that rate of heat generation is uniform across the cell and determined by overpotential and state-of-charge (SoC)-dependent entropic heat sources. In contrast, the heat exchange at the battery surface with the ambient environment depends on temperature, and is therefore not uniform. Contributions from convective and radiation cooling are considered. The model is constructed in COMSOL 3.5a in radial-axial coordinates using the physical cell properties listed in **Tables 1** and **2**. The overpotential η_t and ΔS values are used to calculate heat generation (Equations (2)-(5)). These values are used as input parameter to radial-axial model for the heat generation. Natural heat convection of air around the cell and radiation are taken into consideration knowing that radiation is comparable to natural heat convection amounts. By using Equation (9) at an estimated average temperature of 24˚C (which is estimated according to the experimental measurements of temperature) on the boarder of the cell, h is calculated to be 9 [$W \cdot m^{-2} \cdot K^{-1}$]. The physical properties of the cell and air are assumed to be temperature-independent over a narrow temperature range upon each test which is less than 10˚C and an average extent for each property is chosen. The grid used in the calculations is shown in **Figure 5**.

Equation (1) with initial condition Equation (7) and boundary conditions Equation (8) can then be solved by a time-dependent solver.

3.3. Temperature Profiles

The result of a COMSOL simulation is illustrated in **Figure 6**. As expected, the core temperature of the cell is

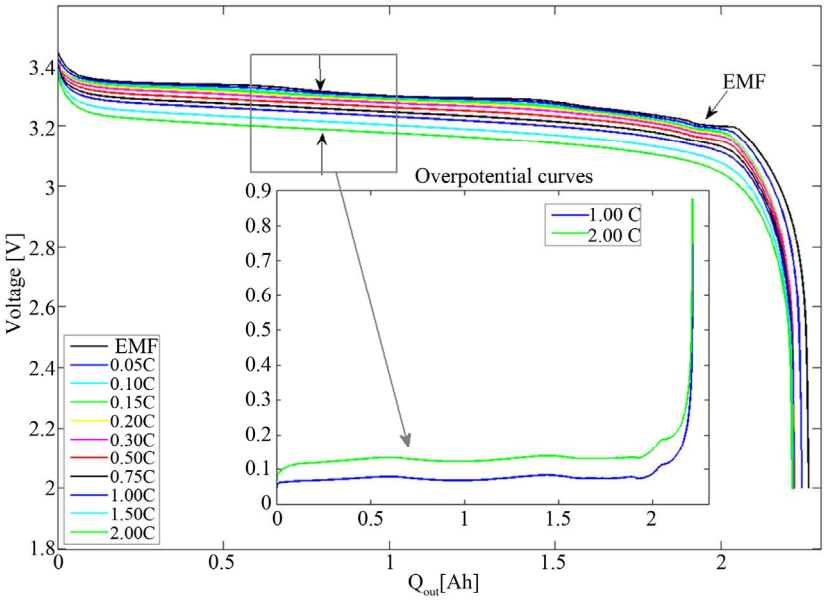

Figure 3. Measured cell potential discharge curves re-plotted as a function of Q_{out}. The extrapolated EMF curve (upper black curve) yields the overpotential curves by subtracting the measured potential curves from the EMF curve (insert).

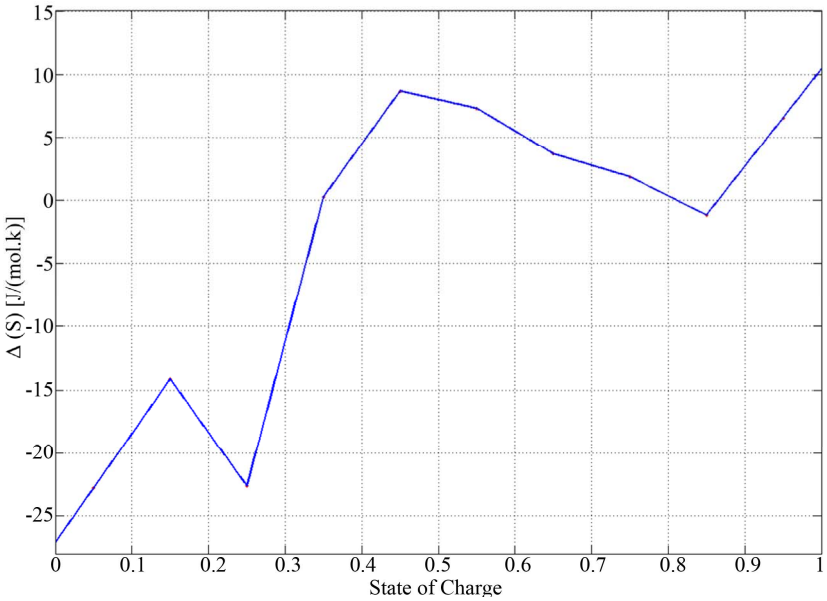

Figure 4. Entropy change values as a function of SoC at 20˚C.

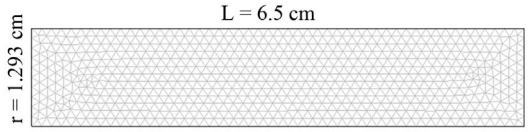

Figure 5. Cell structure and grid.

higher than that at the surface. A maximum temperature of about 28˚C inside the cell is observed at the end of discharge (2 C-rate). Obviously, the edges are coolest with a temperature of approximately 25˚C.

After creating a 2D-COMSOL model it is saved as a MATLAB compatible file (M-file). Then resulting MATLAB function is run in MATLAB, calculating temperature distributions for given set of parameters. These data are used to find the maximum and minimum temperatures upon cycling and plot them simultaneously with the measured temperatures from the experiments to validate the model. The average temperature of the cell is also defined and plotted. To have a better view over the battery operation, the *r-z* surface temperature combined with a colored contour and 1-dimensional time-series tem-

perature plots were calculated, then time-series movie was created. The simulated temperature profiles of the cell at 2C-discharge and upon 3 hours of relaxation in the following period are shown in **Figure 7**. The temperature is measured on the surface of the cell during the experiments, while the heat generation occurs inside the cell. So, it is expected that measurements remain between the minimum and average temperature of the cell. A maximum temperature difference around 3˚C is observed in the cell at the end of discharge. It is seen that even with moderately high discharge rate, which is not extreme case, the core temperature increases by 9˚C.

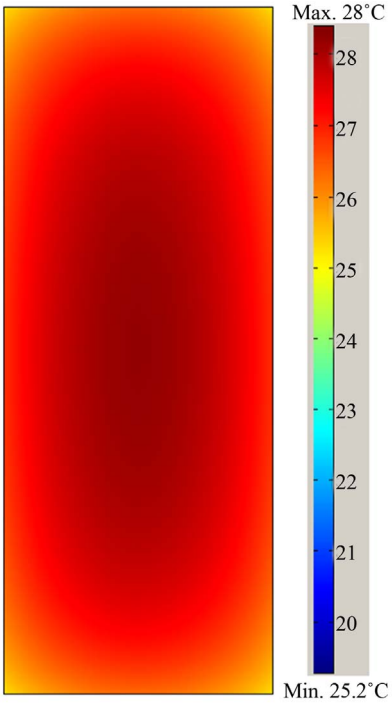

Figure 6. Temperature distribution inside the cell at the end of 2C-rate discharging at an ambient temperature of 20˚C.

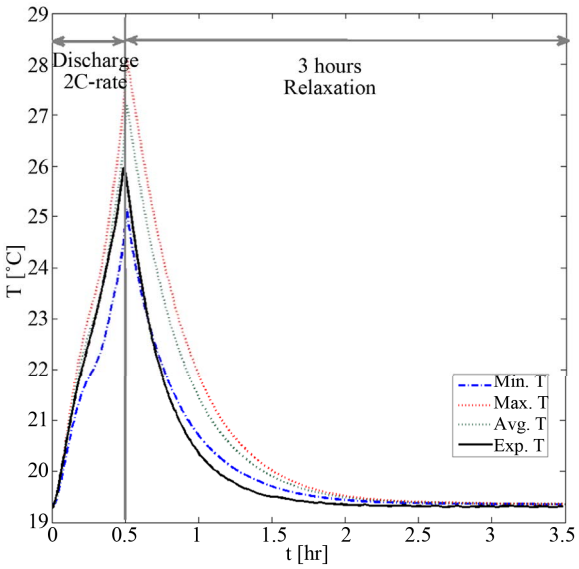

Figure 7. Minimum, maximum and average temperature profiles versus measured temperatures on the surface of the cell at 2C-rate discharge from MATLAB model.

The benefit of running the model in MATLAB is the ability to use it for optimization purposes. Moreover the physical properties of the cell or adjustable parameters for BMS can easily be changed and the results be evaluated individually in-line with other part of the model. To cease or moderate the temperature rise in the cell upon high discharge rates, it is possible to increase the heat transfer coefficient *h*. For instance it is possible to use a fan to apply force convection of air around the cell. On the other hand, heat conduction of the cell seems another limiting factor for effective temperature control over the cell. Therefore it is better to increase the *k* value during manufacturing the cell. A combination of different *k* and *h* values and the consequences on the minimum and maximum temperatures and maximum temperature difference across the cell are presented in **Table 3**. It is concluded that by increasing the thermal conductivity from 0.4 to 2 $W \cdot m^{-1} \cdot K^{-1}$, the gap between the minimum and maximum temperature in the cell decreases from 3˚C to less than 1˚C by running the MATLAB model with the new *k* value. However, it seems that increasing *h* can control the temperature rise. By increasing h by a factor of 4, the maximum internal temperature of the cell decreases to 25.2˚C. However, the maximum temperature difference in the cell increases to 3.9˚C. More effective cooling can be done if the heat transfer coefficient increases, but the heat conduction of the cell decreases.

A 3-dimensional view from the *r*-*z* surface temperature profile and contours and comparison with the maximum temperature at each moment has been plotted in **Figure 8**. The animated movie from the *r*-*z* surface temperature, contours and maximum temperature plot during the whole cycle is available as electronic file.

4. Conclusion

A simple radial-axial model has been developed to evaluate the thermal behavior of $LiFePO_4$ batteries. The overpotential and SoC-dependent entropy change heating are two important sources of heat generation in the cell. The parameter values for these sources are obtained by implementing the previously developed lumped thermal model. The as-determined values for entropy changes are consistent with recent literature [20]. The model provides a good agreement with the experimentally measured temperatures upon cycling. The model is constructed and run in COMSOL 3.5a. It is combined with MATLAB to use optimization capabilities for validating the model with measured data. It is shown that the core temperature of the cell is much higher than that at the surface of the

Table 3. Minimum, maximum and temperature differences for various values of *k* and *h*.

Case	1	2	3	4
k [W·m^{-1}·K^{-1}]	0.4	2	0.4	2
h [W·m^{-2}·K^{-1}]	9	9	45	45
C_p [J·g^{-1}·K^{-1}]	1.36	1.36	1.36	1.36
Results				
Min. T [°C]	25.1	25.5	21.3	22.2
Max. T [°C]	28.0	26.4	25.2	23.4
Max. ΔT [°C]	2.9	0.9	3.9	1.1

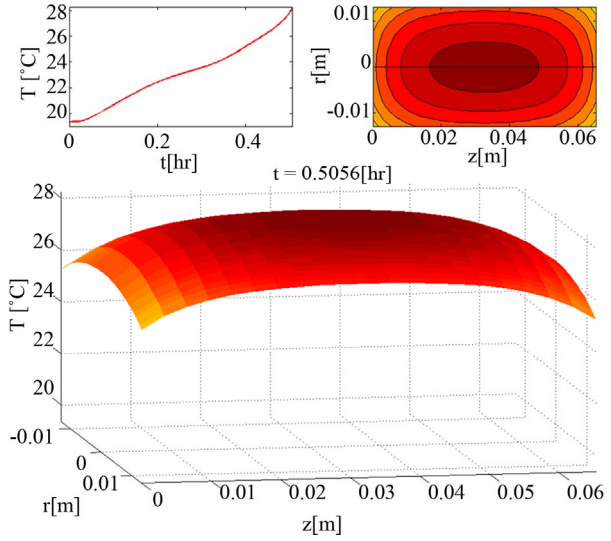

Figure 8. Maximum temperature, surface contour and 3-dimensional temperature distribution of the cell at 2C-rate and end of discharge.

cell. Considering the small diameter of the cell, this is highly important for proper thermal design of larger cells and battery pack design. It was simply illustrated that increasing the heat transfer coefficient can reduce the maximum temperature of the cell, but produce too high temperature difference across the cell. Increasing the thermal conductivity coefficient of the cell during cell manufacturing is also an interesting option to improve the cell properties for efficient thermal management.

REFERENCES

[1] M. S. Rad, D. Danilov, M. Baghalha and M. Kazemeini, *Electrochimical Acta*, Vol. 102, 2013, pp. 183-195.

[2] T. M. Bandhauer, S. Garimella and T. F. Fuller, *Journal of the Electrochemical Society*, Vol. 158, 2011, pp. R1-R25.

[3] L. Song and J. W. Evans, *Journal of the Electrochemical Society*, Vol. 147, 2000, pp. 2086-2095.

[4] W. B. Gu and C. Y. Wang, *Journal of the Electrochemical Society*, Vol. 147, 2000, pp. 2910-2922.

[5] G. G. Botte, V. R. Subramanian and R. E. White, *Electrochimical Acta*, Vol. 45, 2000, pp. 2595-2609.

[6] K. E. Thomas and J. Newman, *Journal of the Electrochemical Society*, Vol. 150, 2003, pp. A176-A192.

[7] K. Smith and Ch. Y. Wang, *Journal of Power Sources*, Vol. 160, 2006, pp. 662-673.

[8] X. Zhang, *Electrochimical Acta*, Vol. 56, 2011, pp. 1246-1255.

[9] L. Cai and R. E. White, *Journal of Power Sources*, Vol. 196, 2011, pp. 5985-5989.

[10] K. Somasundarama, E. Birgerssonb and A. Sadashiv Mujumdara, *Journal of Power Sources*, Vol. 203, 2012, pp. 84-96.

[11] Y. Chen and J. W. Evans, *Journal of the Electrochemical Society*, Vol. 140, 1993, pp. 1833-1838.

[12] Y. Chen and J. W. Evans, *Journal of the Electrochemical Society*, Vol. 141, 1994, pp. 2947-2955.

[13] Y. Chen and J. W. Evans, *Journal of the Electrochemical Society*, Vol. 143, 1996, pp. 2708-2712.

[14] S. Al Hallaj, H. Maleki, J. S. Hong and J. R. Selman, *Journal of Power Sources*, Vol. 83, 1999, pp. 1-8.

[15] K. Onda, H. Kameyama, T. Hanamoto and K. Ito, *Journal of the Electrochemical Society*, Vol. 150, 2003, pp. A285-A291.

[16] H. Yang and J. Prakash, *Journal of the Electrochemical Society*, Vol. 151, 2004, pp. A1222-A1229.

[17] S. C. Chen, C. C. Wan and Y. Y. Wang, *Journal of Power Sources*, Vol. 141, 2005, pp. 111-124.

[18] K. Onda, T. Ohshima, M. Nakayama, K. Fukunda and T. Araki, *Journal of Power Sources*, Vol. 158, 2006, pp. 535-542.

[19] Y. Inui, Y. Kobayashi, Y. Watanabe, Y. Watase and Y. Kitamura, *Energy Conversion and Management*, Vol. 48, 2007, pp. 2103-2109.

[20] Ch. Forgez, D. V. Do, G. Friedrich, M. Morcrette and Ch. Delacourt, *Journal of Power Sources*, Vol. 195, 2010, pp. 2961-2968.

[21] D. H. Jeon and S. M. Baek, *Energy Conversion and Management*, Vol. 52, 2011, pp. 2973-2981.

[22] D. Danilov, A. Lyedovskikh and P. H. L. Notten, 7*th International IEEE Vehicle Power and Propulsion Conference*, Chicago, 6-9 September 2011.

[23] S. W. Churchill and H. H. S. Chu, *International Journal of Heat Mass Transfer*, Vol. 18, 1975, p. 1049.

[24] V. Pop, H. J. Bergvard, D. Danilov and P. H. L. Notten, "BMS: Accurate State-of-Charge Indication for Battery-Powered Applications," Springer, New York, 2008.

[25] D. Danilov, R. Niessen and P. H. L. Notten, *Journal of the Electrochemical Society*, Vol. 158, 2011, pp. A215-A222.

